

## Article

# Optimization Configuration of Grid-Connected Inverters to Suppress Harmonic Amplification in a Microgrid

Xing Sun, Wanjun Lei \*, Yuqi Dai, Yilin Yin and Qian Liu

School of Electrical Engineering, Xi'an Jiaotong University, Xi'an 710049, China; sunxingdc@126.com (X.S.); daiqi@163.com (Y.D.); yyl19990513@stu.xjtu.edu.cn (Y.Y.); qianliu1998@foxmail.com (Q.L.)

\* Correspondence: leiwanjun@mail.xjtu.edu.cn

**Abstract:** This paper provides insight into the optimal configuration scheme of the grid-connected inverters based on harmonic amplification suppression. The connection of the inverters changes the natural resonance frequencies of the grid. Hence, a reasonable configuration of grid-connected inverters can optimize the impedance distribution and shift the natural resonance frequencies to frequency bands farther away from the harmonic sources. We proposed a scheme of site selection and determination of the number of inverters to suppress harmonic amplification. The resonance frequencies and modal frequency sensitivities (MFSs) were obtained by the resonance modal analysis (RMA). Moreover, the concepts of security region and insecurity region of resonance frequency were illustrated. The grid-connected sites can be obtained by calculating the participation factors (PFs) of the resonance frequencies in the insecurity region. Furthermore, the optimal number was determined by building the Norton equivalent circuit of the inverter and evaluating the output impedance at each frequency. Finally, simulations in Matlab/Simulink based on a modified IEEE-9 bus microgrid were utilized to verify the effectiveness of the proposed scheme.

**Keywords:** grid-connected inverters; harmonic amplification; impedance distribution; resonance modal analysis (RMA); optimization; output impedance



**Citation:** Sun, X.; Lei, W.; Dai, Y.; Yin, Y.; Liu, Q. Optimization

Configuration of Grid-Connected Inverters to Suppress Harmonic Amplification in a Microgrid.

*Energies* **2022**, *15*, 4989. <https://doi.org/10.3390/en15144989>

Academic Editor: Nicu Bizon

Received: 22 May 2022

Accepted: 3 July 2022

Published: 7 July 2022

**Publisher's Note:** MDPI stays neutral with regard to jurisdictional claims in published maps and institutional affiliations.



**Copyright:** © 2022 by the authors. Licensee MDPI, Basel, Switzerland. This article is an open access article distributed under the terms and conditions of the Creative Commons Attribution (CC BY) license (<https://creativecommons.org/licenses/by/4.0/>).

## 1. Introduction

The high-density access of many nonlinear loads causes severe harmonic pollution in the grid [1–3]. Even though a single nonlinear load can be regarded as a micro harmonic source, the superposition of a multitude of micro harmonic sources can have significant effects on the grid. Therefore, the harmonic pollution of modern power networks presents the characteristics of high density, decentralization, and whole network [4–6]. On the other hand, the grid-connected power generation technology of distributed power generation (DPG), such as wind and photovoltaic power generation, has attracted increasing attention [7,8]. In a microgrid containing DPG, the structure of multiple inverters connected in parallel is usually adopted [9]. Multiple inverters are connected to microgrids, and the impedance distribution is affected. An unreasonable grid connection may make the impedance distribution of the grid match with the harmonic source and further strengthen the harmonic amplification. Harmonic amplification causes the degradation of power quality, leading to system instability and threatening the system's security and stability [10,11].

Existing methods of suppressing harmonic amplification are provided in [12–20]. They can be divided into the following two categories: reducing the harmonic injection and breaking the requisite of harmonic amplification. Reducing the harmonic injection mainly includes controlling the harmonic sources and harmonic compensation. Active control of harmonic sources can reduce harmonic excitation by improving the topology and control of power electronic equipment [12], e.g., multipulse AC–DC converters [13] and power factor correction [14]. However, they are unsuitable for industrial applications due to their limited capacity, cost, and reliability. Harmonic compensation requires the installation of harmonic

compensation devices near nonlinear loads. Harmonic compensation devices include passive power filters [15], active power filters [16,17], and hybrid active power filters [18]. However, these filters bring about new resonances. In particular, when connected to a weak grid, they can significantly reduce system stability [19]. To break the requisite of harmonic amplification, it is desired to move harmonics to frequencies where there is no harmonic source or a harmonic source with a minimal value [20]. This method can be realized by installing passive devices or active devices at critical nodes, and it has the characteristics of low cost and good adaptability. This paper studied this method based on the connection of inverters.

At present, the optimization objectives of grid-connected studies of DPG are to improve the reliability of the distribution system [21], minimize power loss [22,23], and improve voltage stability [24,25]. However, when the output impedance of the inverter cannot be ignored, the grid connection of DPG will change the topology and impedance distribution of the grid, especially when multiple inverters are connected in parallel [26]. Therefore, it is necessary to reasonably configure the inverters to optimize the impedance distribution, keep the resonance frequency away from the harmonic source, improve the voltage quality and prevent potential resonance.

The traditional resonance method of the power system is the frequency scan method [27]. The resonance modal analysis (RMA) method was first proposed in [28] to analyze the harmonic resonance mechanism. It overcomes the shortcomings of the frequency scan method, such as limited detection range, complicated analysis and calculation, and the inability to provide more relevant information to solve the resonance problem. Later on, in [29], RMA was applied to solve the resonance problem in railway electrification systems.

This paper presents a grid-connected optimization scheme of inverters to suppress harmonic amplification in a microgrid. Resonance frequency was identified based on RMA and critical sites were determining based on the participation factor (PF). The number of connected inverters was optimized by calculating the modal frequency sensitivities (MFSs) of the components. Based on the quasi-proportional resonance controller, the Norton equivalent model of an inverter considering capacitor current feedback was established. Calculation of the output impedance at resonance frequency was conducted, verifying consistent impacts on the impedance distribution from the inverter and equivalent passive components. The security region and insecurity region of resonance frequency were discussed. By optimizing the configuration of the inverters, the resonance frequency can be maintained in the security region to reduce the harmonic impedance in the insecurity region and reduce the voltage distortion. In addition, simulation results are provided to validate the theoretical analysis, followed by the conclusion of the main contributions of this paper.

## 2. Resonance Modal Analysis Method

### 2.1. Identification of Resonance

The basic principle of the RMA is as follows. For an  $n$ -node network, the occurrence of harmonic resonance means that the network node admittance matrix has become or is close to becoming a singular matrix. The characteristic of a singular matrix is that the eigenvalue of zero appears, so when a matrix is close to singular, the inverse of its eigenvalues or the eigenvalues of its inverse matrix will tend to infinity. Because zero eigenvalues are the fundamental characteristic of resonance, the mode of harmonic resonance can be accurately defined according to the eigenvalue change.

Assuming that harmonic resonance occurs at a particular frequency  $f$ , the nodal admittance matrix is a singular matrix. The node injection current is represented by  $[I]_f$  where all elements are finite values, and the node voltage vector  $[V]_f$  at the resonance frequency is [28]

$$[V]_f = [Y]_f^{-1}[I]_f \quad (1)$$

where  $[Y]_f$  is the network admittance matrix. Here, some elements in  $[Y]_f$  are infinite. The admittance matrix can be represented as

$$[Y]_f = [L]_f[\Lambda][T]_f \quad (2)$$

where  $\Lambda = \text{diag}(\lambda_1, \lambda_2, \dots, \lambda_n)$  is the diagonal eigenvalue matrix of  $Y$ . The reciprocal of the eigenvalue characterizes the impedance property, defined as “modal impedance”.  $L$  and  $T$  are the left and right eigenvector matrices, respectively. The location with the most significant PF is the center of resonance. PF can be obtained by [28]

$$\text{PF}_{bm} = L_{bm}T_{mb} \quad (3)$$

where  $b$  is the bus number and  $m$  is the node number. Generally, installing devices at the resonance center to adjust the impedance distribution has the most noticeable effect and can reduce the impact on other resonance frequencies.

## 2.2. Modal Frequency Sensitivity

Although the center of resonance can be determined based on the PF, the influence of specific component parameters on resonance cannot be determined. The introduction of a sensitivity analysis in [30] is conducive to the influence analysis of parameters on system resonance. It provides a basis for the treatment of harmonic resonance and the design of component parameters.

The eigenvalue sensitivity to  $Y_{ij}$  is calculated as

$$S_{m,ij} = \frac{\partial \lambda_m}{\partial Y_{ij}} = T_{mi}L_{jm} \quad (4)$$

where  $\lambda_m$  is the  $m$ th eigenvalue of matrix  $Y$ , and  $t_{mi}$  and  $l_{jm}$  are the  $m$ th-row  $i$ th-line entry of the matrix and  $j$ th-row  $m$ th-line entry, respectively.

Assuming that

$$\lambda_m = \lambda_r + j\lambda_i \quad (5)$$

$$S_{\lambda,ii} = S_r + jS_i. \quad (6)$$

The impedance sensitivity of admittance  $Y = G + jB$  can be calculated as

$$\frac{\partial |\lambda_m|}{\partial G} = \frac{S_r \lambda_r + S_i \lambda_i}{|\lambda_m|} = u \quad (7)$$

$$\frac{\partial |\lambda_m|}{\partial B} = \frac{S_r \lambda_i - S_i \lambda_r}{|\lambda_m|} = v. \quad (8)$$

The MFS index is derived as [30]

$$\frac{df}{d\alpha} = -\frac{\Delta f}{\Delta \alpha} = -\frac{\frac{\partial^2 |\lambda_m|}{\partial f \partial \alpha}}{\frac{\partial^2 |\lambda_m|}{\partial^2 f}} \quad (9)$$

$\partial^2 |\lambda_m| / \partial \alpha \partial f$  can be calculated as

$$\frac{\partial^2 |\lambda_m|}{\partial f \partial \alpha} = \frac{\partial u}{\partial f} \frac{\partial G}{\partial \alpha} + u \frac{\partial^2 G}{\partial \alpha \partial f} + \frac{\partial v}{\partial f} \frac{\partial B}{\partial \alpha} + v \frac{\partial^2 B}{\partial \alpha \partial f} \quad (10)$$

$\partial G/\partial\alpha$ ,  $\partial^2 G/\partial\alpha\partial f$ ,  $\partial B/\partial\alpha$ , and  $\partial^2 B/\partial\alpha\partial f$  can be obtained using a series resistor–inductor–capacitor branch [29]. The second-order derivative of the eigenvalue magnitude to frequency  $f$  can be derived during the frequency scan process as follows:

$$\frac{\partial^2 |\lambda_m|}{\partial f^2} = \frac{1}{4\Delta f^2} (|\lambda_m|^{f+2\Delta f} + |\lambda_m|^{f-2\Delta f} - 2|\lambda_m|) \quad (11)$$

Combined with the MFSs of component parameters and the equivalent output impedance of the inverter, the impedance distribution after connecting the inverters can be easily understood. Therefore, the number of connected inverters can be optimized after the suitable sites are determined.

### 3. Output Impedance Characteristics of the Inverter

This section discusses the inverter's control and topology and establishes the corresponding Norton equivalent circuit. The feasibility of connecting the inverter to optimize the microgrid impedance is discussed by analyzing the output impedance characteristics of the inverter at different frequencies.

#### 3.1. Equivalent Circuit of the Inverter

The structure diagram of a single three-phase LCL grid-connected inverter is shown in Figure 1. The upper part is the power circuit configuration, and the lower is the control structure diagram.  $U_{dc}$  is the DC bus voltage obtained through the DC voltage stabilizing link, and  $U_{inv}$  is the output voltage of the inverter.  $C$  is the filter capacitance.  $L_1$  and  $L_2$  are the inverter-side and grid-side filter inductance, respectively.  $i_{inv}$ ,  $i_2$  and  $i_c$  are the inverter-side current, grid-side current and filter-capacitor current, respectively.  $U_{PCC}$  is the voltage of the point of common coupling (PCC).  $i_{ref}$  is the filter output reference current of the inverter.  $U_g$  is the grid voltage. In this paper, closed-loop control was adopted for the current control, and proportional feedback control was adopted for the active damping link.

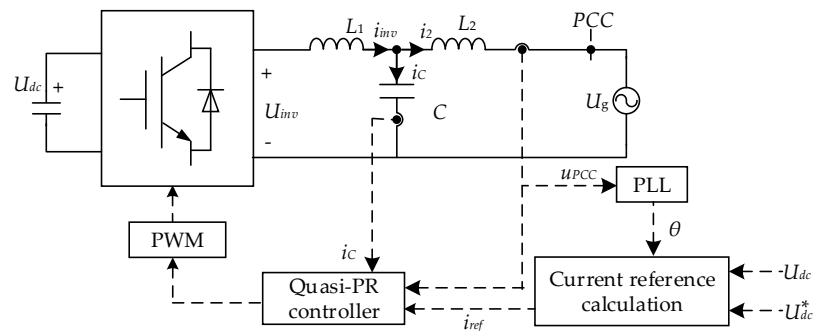


**Figure 1.** System structure of single-phase grid-connected inverter with LCL filter.

Figure 2 shows the control block diagram of the current control and active damping link of the inverter filter system, in which  $K_{pwm}$  is the gain of the inverter. Quasi-proportional resonance (QPR) control was adopted for the current controller, and the expression is as follows:

$$G_{PR}(s) = K_p + \frac{K_r \omega_c s}{s^2 + 2\omega_c s + \omega_0^2} \quad (12)$$

where  $K_p$  and  $K_r$  are the proportionality coefficient and resonance coefficient, respectively;  $\omega_c$  is the cut-off frequency;  $\omega_0$  is the fundamental angular frequency. To ensure the influence of active damping on the peak value of the natural resonance amplitude–frequency response of the filter, the proportional feedback link based on  $K_C$  is added to the forward channel of the quasi-proportional resonance control output link.

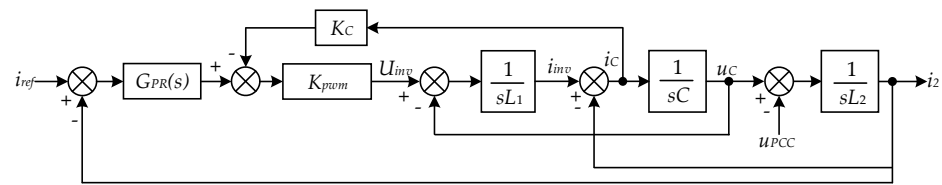


Figure 2. The control diagram of the current and damping control loop.

According to the control block diagram shown in Figure 2, the Norton equivalent circuit of the inverter shown in Figure 1 can be obtained (see Figure 3). The equivalent current and equivalent admittance are  $I_{eq}(s)$  and  $Y_{eq}(s)$ , respectively. Their expressions are shown in (13) and (14).

$$I_{eq}(s) = \frac{K_{pwm}G_{PR}(s)}{L_1L_2Cs^3 + K_{pwm}K_cL_2Cs^2 + (L_1 + L_2)s + K_{pwm}G_{PR}(s)} i_{ref} \tag{13}$$

$$Y_{eq}(s) = \frac{L_1C_f s^2 + K_{pwm}K_c C_f s + 1}{L_1L_2C_f s^3 + K_{pwm}K_c L_2C_f s^2 + (L_1 + L_2)s + K_{pwm}G_{PR}(s)} \tag{14}$$

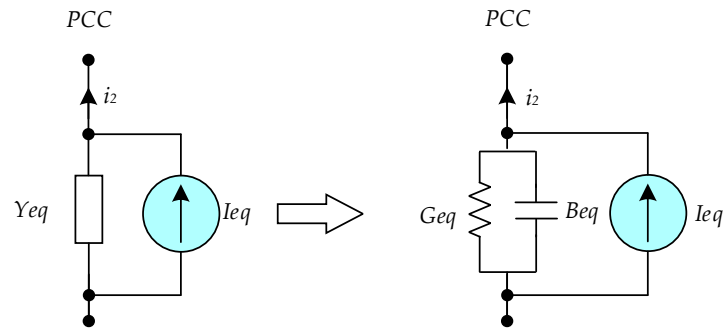


Figure 3. Norton equivalent circuit of the three-phase inverter.

The grid-connected inverters can change the self-admittance of PCCs and thus change the impedance distribution. To reduce the installation cost and capacity, this paper chose to connect the inverters to the site with high MFS, namely the site with a significant PF.

### 3.2. Output Impedance of the Inverter

It can be seen from (14) that the output impedance of the inverter is not a constant but changes with frequency. This section discusses the output impedance characteristics of the inverter and the influence of the connection on the distributed impedance. The parameters of the inverter are shown in Table 1.

Table 1. Control and electrical parameters of the inverter.

Symbol	Instruction	Values
$K_p$	proportionality coefficient	0.4
$K_r$	resonance coefficient	200
$\omega_c$	cut-off frequency	5
$K_c$	capacitor-current feedback constant	1
$L_1$	Inverter-side filter inductor	4 mH
$L_2$	Grid-side filter inductor	0.5 mH
$C$	Filter capacitor	20 $\mu$ F
$f_0$	Grid frequency	50 Hz
$U_{DC}$	DC voltage	700 V

Assume that

$$Y_{eq}(s) = G_{eq}(s) + jB_{eq}(s) \tag{15}$$

where  $G_{eq}(s)$  and  $B_{eq}(s)$  are the equivalent conductance and equivalent susceptance, respectively. The effect of frequency on  $G_{eq}$  and  $B_{eq}$  is depicted in Figure 4.

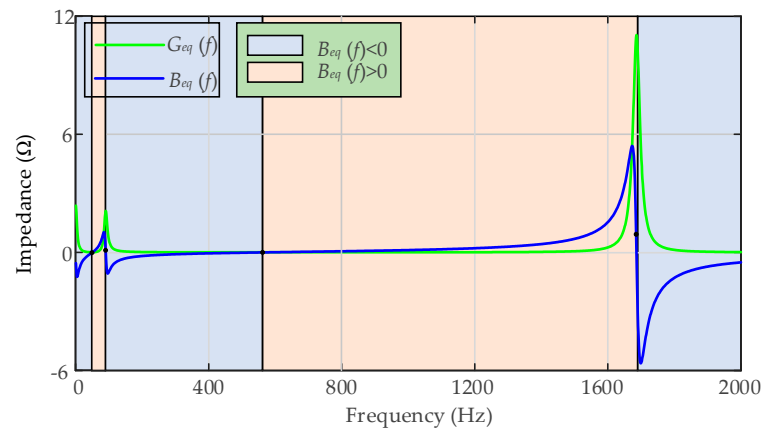


Figure 4. Effect of frequency on  $G_{eq}(f)$  and  $B_{eq}(f)$ .

Within the range of (0, 49 Hz), (91 Hz, 562 Hz) and (1686 Hz, 2000 Hz),  $B_{eq}$  is less than 0. The output impedance of the inverter is inductive and is equivalent to the parallel connection of a  $1/G_{eq}$  resistor and a  $1/(\omega \times B_{eq})$  ( $\omega = 2\pi f$ ) inductor. Within the range of (50 Hz, 90 Hz) and (562 Hz, 1685 Hz),  $B_{eq}$  is larger than 0. The output impedance of the inverter is capacitive and can be equivalent to the parallel connection of a  $1/G_{eq}$  resistor and a  $B_{eq}/\omega$  capacitor.

The equivalent capacitor value  $C_{eq}$  and inductance value  $L_{eq}$  are shown in Figure 5. In the low-frequency and high-frequency bands, the output impedance of the inverter is almost inductive, while in the medium-frequency band, it is capacitive. Except at the junction of different parts,  $C_{eq}$  and  $L_{eq}$  change slightly. Notably,  $G_{eq}$  always has a small value, so it has little effect on PCC self-admittance. The impedance distribution of the grid is mainly affected by  $B_{eq}$ .

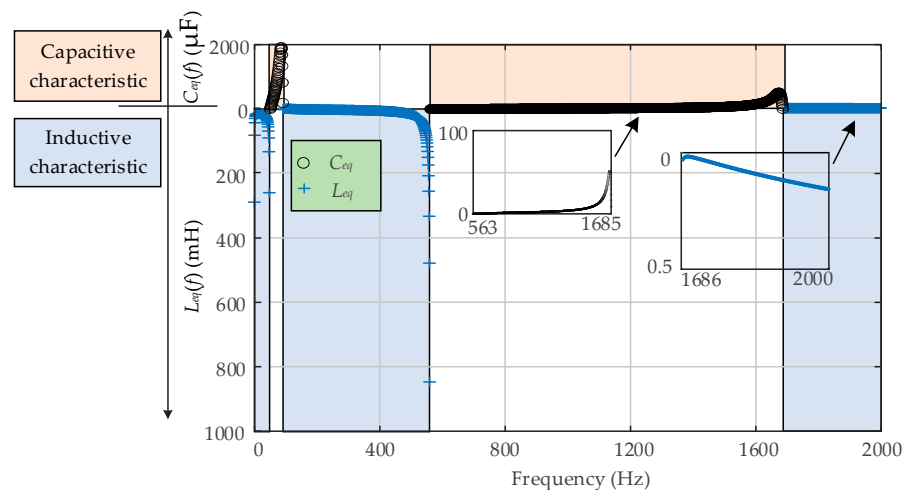


Figure 5. Effect of frequency on  $C_{eq}$  and  $L_{eq}$ .

### 3.3. Effect of Grid-Connected Inverter on Impedance Distribution

It can be seen from Figure 5 that, in each frequency band greater than 90 Hz, the  $C_{eq}$  or  $L_{eq}$  is an approximately constant value  $C_{eq}(f_0)$  (or  $L_{eq}(f_0)$ ) ( $f_0$  is a specific frequency in this frequency band). Therefore, in a specific frequency range, the impedance distribution of connecting the inverter is consistent with that of connecting the passive components with the same equivalent capacitance (or inductance). The IEEE 9-bus system was studied in this paper to verify its consistency [31]. The network topology is shown in Figure 6.

There are three generators and three loads; generator  $G_1$  is the balance node, and the rest are PV nodes. The loads were modelled as the constant power loads. To facilitate the inverters' connection, the test system's voltage and power were scaled down to 230 V and 100 kW, respectively. The scanning frequency  $\Delta f$  for RMA was set to 5 Hz. The resonance mode information of the test system is shown in Figure 7, and there were six resonance frequencies of 305, 420, 435, 590, 760 and 825 Hz. The equivalent output impedance of the inverter was inductive at  $f = 305$  Hz and capacitive at  $f = 760$  Hz. These two resonance frequencies were selected to verify the consistency.

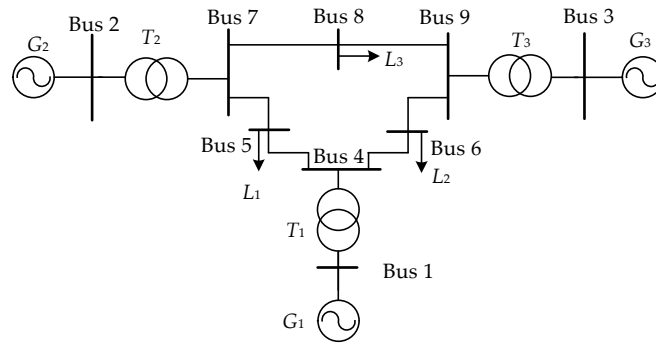


Figure 6. IEEE 9-bus regional microgrid.

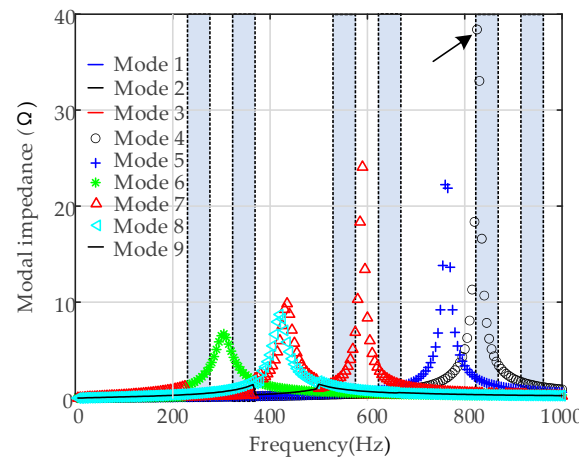


Figure 7. Modal impedances of the test system.

The effect of buses' parameters on the resonance can be clearly understood for the PF information shown in Figure 8. The PFs of buses 1, 2, and 3 were all zero, which means that changing their parameters did not affect the resonance frequencies. This is because buses 1, 2 and 3 were connected with voltage sources. Their self-admittances are infinite, and changing the parameters of the components did not change their self-admittances. The resonance centers of  $f = 305$  Hz and  $f = 760$  Hz were bus 6 and 8, respectively. They had the most significant PFs at the corresponding resonance frequencies and were selected as the connection sites. The equivalent output impedance of the inverter at  $f = 305$  Hz and  $f = 760$  Hz can be obtained by (11), which are  $Y_{eq}|_{f=304\text{ Hz}} = (0.0092 - j0.091) \Omega$  and  $Y_{eq}|_{f=760\text{ Hz}} = (0.0051 + j0.049) \Omega$ , respectively.

The mode impedance diagram of the test system connecting the inverters and the passive branches is shown in Figure 9. It is obvious that connecting the inverter and the passive branch produces almost the same effect. Their curves have the same trend, and their resonance frequencies are almost the same. For example, the resonance frequencies of the system where the inverter is connected to bus 6 and where the passive branch of  $(0.0092 - j0.091)$  is connected to bus 6 are both 309 Hz.

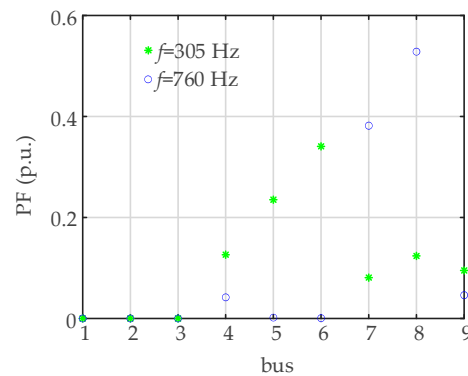


Figure 8. PFs corresponding to resonance frequencies  $f = 305$  Hz and  $f = 760$  Hz.

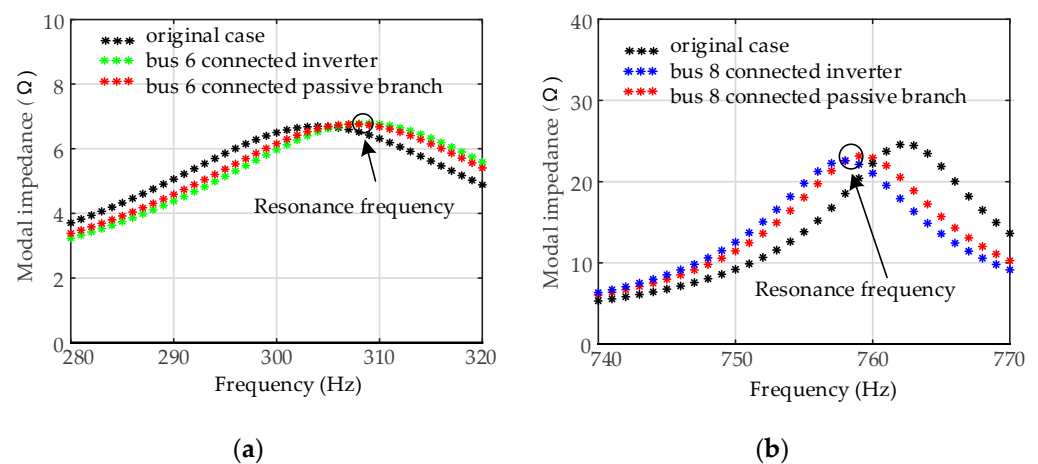


Figure 9. Effect of components on the resonance mode of: (a)  $f = 305$  Hz; (b)  $f = 760$  Hz.

From the aforementioned analysis, it can be seen that the optimal connection number of the inverters can be obtained by calculating the MFS of the  $C_{eq}$  (or  $L_{eq}$ ). In addition, the resonance frequency needs to be calculated by RMA again to correct the error.

#### 4. Connection Optimization Scheme of Inverter

##### 4.1. Concept of Security Region

Harmonic amplification is caused by matching the harmonic sources with the natural resonance frequencies of the grid. In other words, harmonic amplification can be avoided by keeping the natural resonance frequencies away from the frequency of the harmonic sources instead of weakening the harmonic sources. In addition, harmonic source frequencies often show a specific regularity. For example, harmonic source frequencies of the power-electronic grid are generally  $6k \pm 1$  ( $k = 1, 2, \dots, n$ ). When the natural resonance frequencies are far from the harmonic source frequencies, such as  $(6k \pm 3)$ , it can be said that these frequencies can be regarded as “safe”. Conversely, frequency ranges close to the harmonic source frequencies are “unsafe”.

The driving point impedance of a specific node is shown in Figure 10.  $f_1, f_2$ , and  $f_3$  are all harmonic source frequencies, and  $f_{res1}$  and  $f_{res2}$  are the natural resonance frequencies of the grid. The shaded areas are the insecurity regions, and the blank parts are the security regions. No treatment is required if the resonance frequency is in the security region, such as  $f_{res2}$ . If it is in the insecurity region, such as  $f_{res1}$ , it needs to be shifted to the security region using external methods.

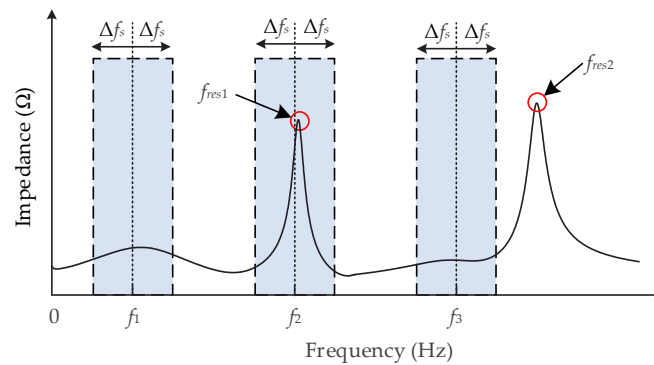


Figure 10. Diagram of the driving point impedance.

#### 4.2. Study on Optimization Scheme

By optimizing the connection sites and number of inverters, the harmonic amplification can be suppressed, and the potential of resonance can be reduced. The proposed optimization process can be summarized as follows:

Step 1: Use RMA to calculate resonance frequencies and PFs of frequencies ( $f_{res1}, f_{res2}, \dots, f_{res3}$ ) in the insecurity regions.

Step 2: To reduce the influence on other resonance frequencies, use site with the significant PF as the location of the grid-connected inverters.

Step 3: Calculate the equivalent inductance  $C_{eq}$  or equivalent capacitance  $L_{eq}$  of the inverter at  $f = f_{resi}$ .

Step 4: Calculate the MFS to  $C_{eq}$  or  $L_{eq}$  and the number of inverters  $m$  required to shift it to the security region. The  $m$  should satisfy:

$$\frac{\partial f_{resi}}{\partial C} \cdot m \cdot C_{eq}(f_{resi}) + f_{resi} \in (f_{secmin}, f_{secmax}) \quad (16)$$

where  $f_{secmin}$  and  $f_{secmax}$  are lower- and upper-frequency limits of the security region, respectively.

Step 5: Connect  $m$  inverters and calculate the resonance frequency. If it is in the security region, the solution is reached; otherwise, proceed to Step 1.

The proposed optimization scheme is presented in Figure 11.

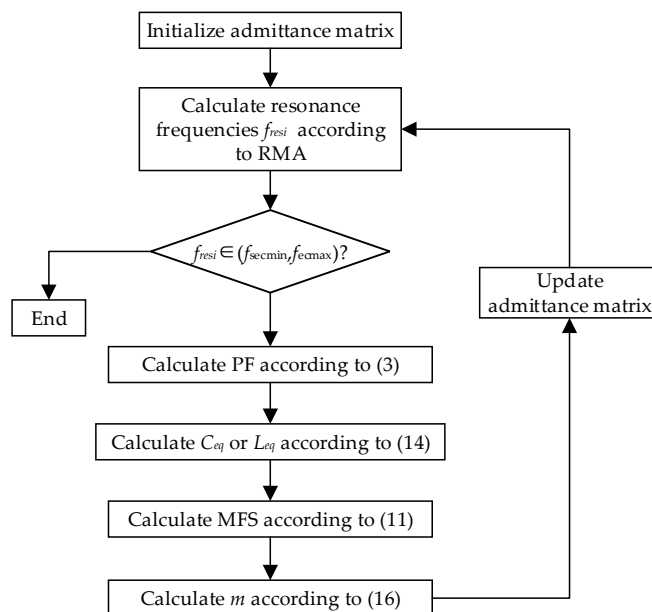


Figure 11. Flow chart of the optimization for grid-connected inverters.

## 5. Simulation Verification

The modified IEEE 9-bus microgrid was used to verify the proposed scheme. To characterize the dispersed harmonics generated by power electronic devices, harmonic sources were set at the three load-connected sites of bus 5, bus 6 and bus 8. The current information of harmonic sources is shown in Table 2.  $\Delta f_s$  was set to 25 Hz. All inverters had the same parameters, as shown in Table 1. The modal impedance diagram of the test system is shown in Figure 7.

**Table 2.** Node harmonic current injection orders and sizes.

Harmonic Source Order h (p.u.)	Bus 5 (A)	Bus 6 (A)	Bus 8 (A)
5	11.2	10.3	10.0
7	10.6	8.5	9.0
11	8.6	7.3	7.5
13	8.9	7.1	9.2
17	7.0	6.8	5.7
19	6.4	7.1	4.5

Figure 12 demonstrates that only  $f = 825$  Hz was in the insecurity region (825 Hz, 875 Hz). The output impedance at  $f = 825$  Hz can be calculated as  $Y_{vsc}|_{f=825 \text{ Hz}} = (0.0054 + j0.0655) \Omega$ . It is capacitive, and the equivalent capacitance  $C_{eq}$  is  $12.64 \times 10^{-6}$  F. The PF distribution of the resonance frequency is shown in Figure 11. Bus 4 has the largest PF at this resonance frequency, while the PFs of other nodes are close to zero. Bus 4 is the resonance center of this resonance frequency and is the optimal place to install the inverters.

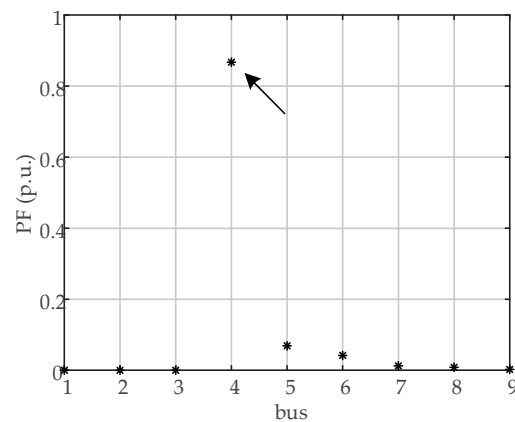


**Figure 12.** PFs corresponding to the resonance frequency  $f = 825$  Hz.

$G_{eq}$  has a slight effect on the self-admittance of PCC, and the impedance distribution of the grid is mainly affected by  $C_{eq}$ . Therefore, only the MFS to  $C_{eq}$  needs to be calculated. The MFS to  $C_{eq}$  on bus 4 can be obtained by (14), which is  $\partial f_{res}/\partial C = -6.64 \times 10^5$  Hz/F. By (16), after connecting an inverter, the new resonance frequency is  $f_{res} - C_{eq} \times \partial f_{res}/\partial C = 819$  Hz. The resonance frequency is already in the security region, but it is still close to the insecurity region. To further reduce the voltage distortion and increase the “safety” margin when the impedance distribution varies, the number of inverters should be further optimized. When three inverters are connected, the resonance frequency is reduced to 801 Hz and is far from the insecurity region. The modal impedance information with three inverters connected is shown in Figure 13. It can be seen that all resonance peaks are in the security region. The resonance frequency after shifting calculated by RMA is 800 Hz and is basically consistent with the theoretical value.

A corresponding model of the test system was developed in Matlab/Simulink and the obtained results were compared with the theoretical analysis. When bus 4 was connected to different numbers of inverters, the voltage distortion information of the bus was obtained which is shown in Figure 14. As the number of connected inverters increased, the total

harmonic distortion (THD) of  $U_4$  gradually decreased. The THD of the original case is 7.06%, and after connecting one, two, and three inverters it was 5.07%, 3.86%, and 3.18%, respectively. The voltage spectra information of bus 4 with different numbers of inverters is shown in Figure 15. After optimization, the magnitude of the 17<sup>th</sup> voltage harmonic decreased significantly, whereas the amplitude of the other harmonics changed slightly. Notably, when more inverters were connected, the THD still reduced, but not significantly. Even if 15 inverters are connected, the THD is only reduced to 2.17%. This means that the optimized THD has a lower limit, and a specific number of connected inverters meets the requirements.

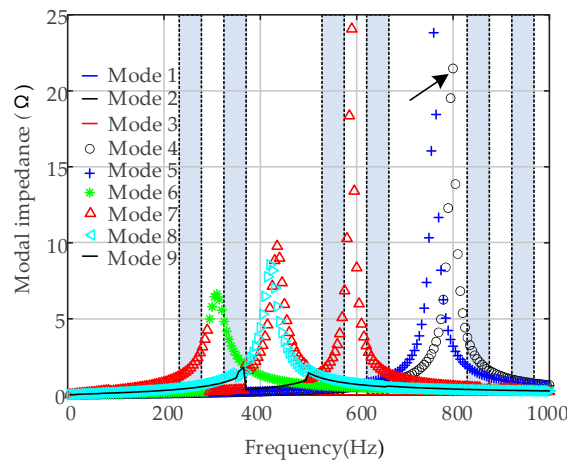


Figure 13. Modal impedances of the test system with three inverters on bus 4.

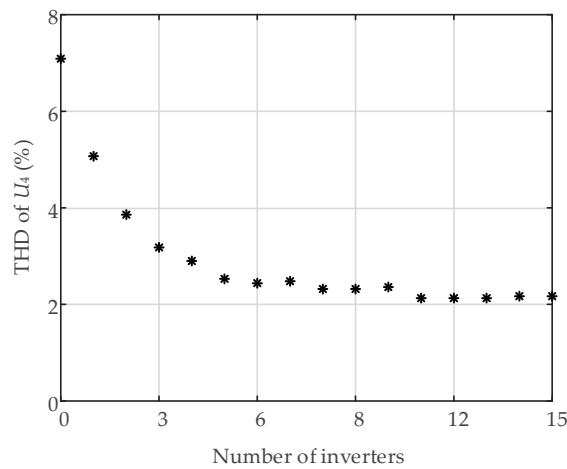


Figure 14. Effect of the number of inverters on THD of  $U_4$ .

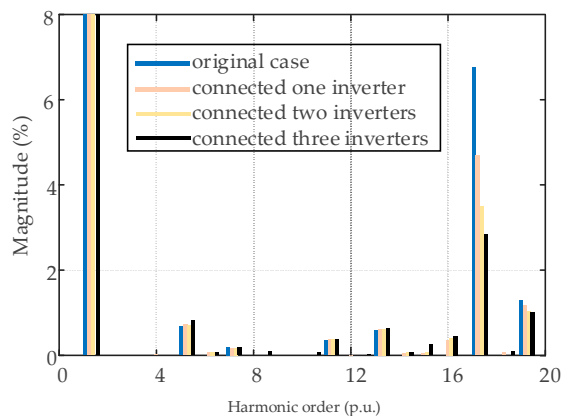


Figure 15. Voltage spectra of bus 4 connected with different numbers of inverters.

The impedance scanning diagram of the test system with bus 4 connected to three inverters is shown in Figure 16. It clearly shows that the driving point impedance of the insecurity region significantly reduced. The waveform of optimized  $U_4$  obviously improved (see Figure 17a). Since the PFs of other nodes were very small, the connection of inverters at bus 4 had little effect on the voltage waveform of other buses (see Figure 17b–f).

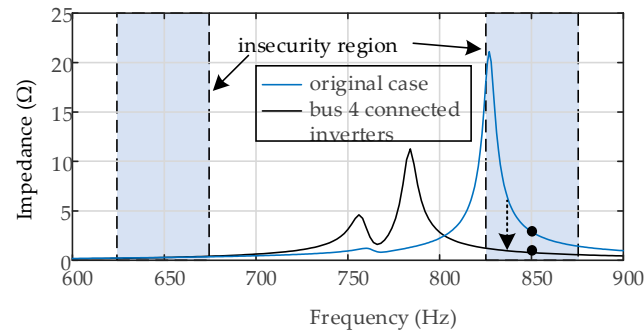


Figure 16. Frequency scan diagram of bus 4.

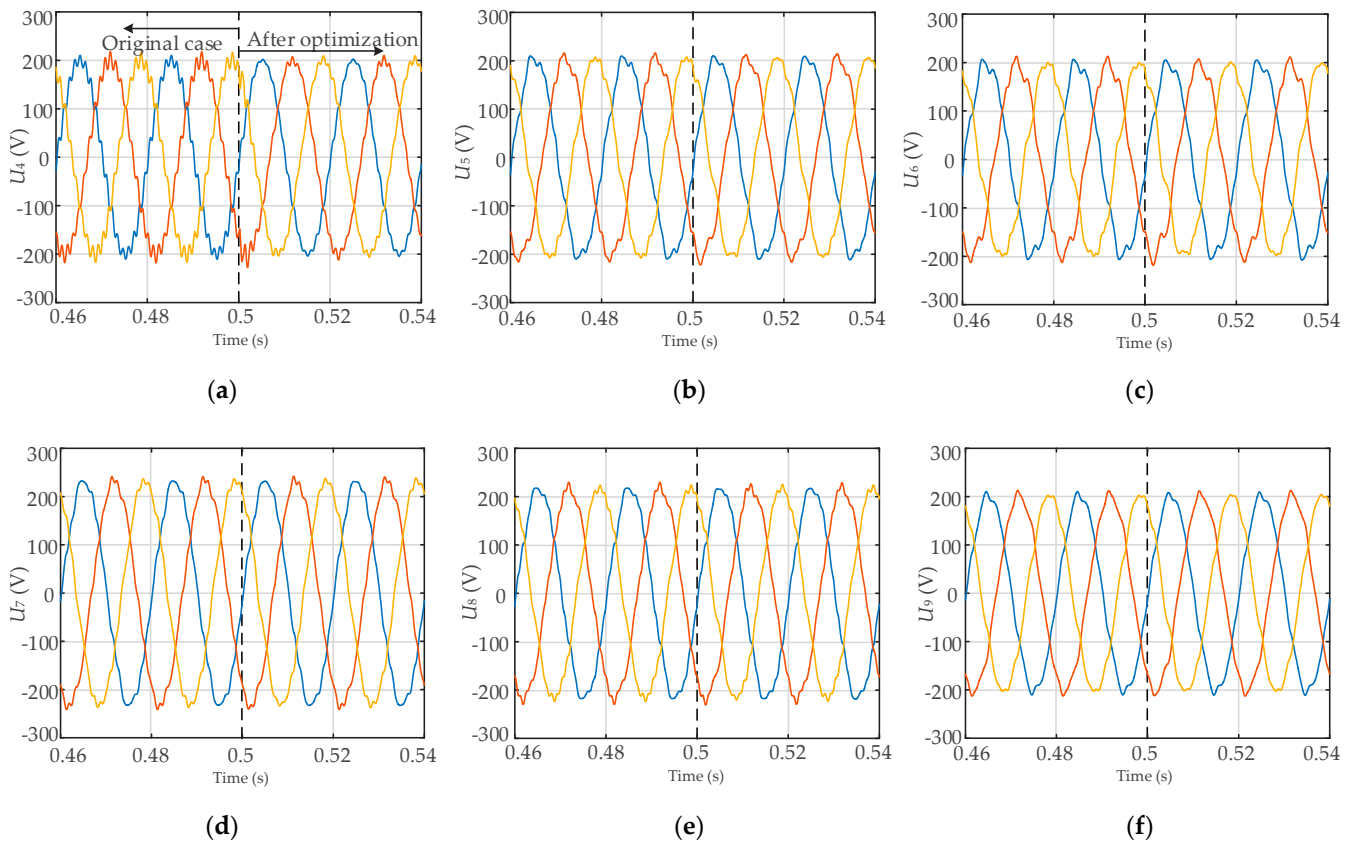
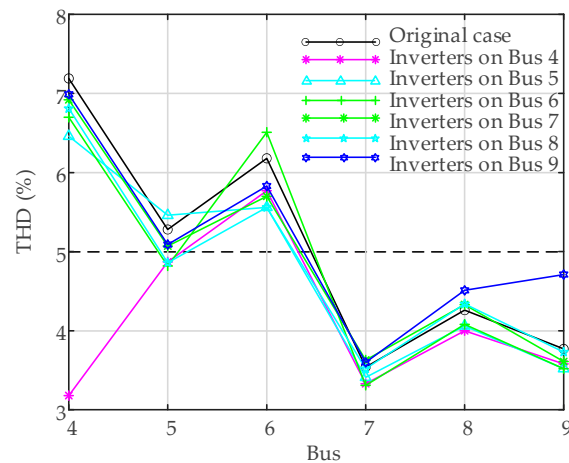


Figure 17. The voltage waveform of the original case and after optimization. (a) bus 4. (b) bus 5. (c) bus 6. (d) bus 7. (e) bus 8. (f) bus 9.

Figure 18 and Table 3 show the THD information when three inverters were connected at different buses. It can be clearly seen that when the inverters were installed at bus 4, the THD of  $U_4$  significantly reduced, and the THDs of other node voltages also slightly reduced. However, when inverters were connected to other nodes, it had little impact on the voltage of each node and even further worsened the original voltage quality. For example, in the original case, the THD of  $U_9$  was 3.77%. When node 9 is connected to the inverter, the THD rises to 4.71%.



**Figure 18.** Voltage distortion when inverters are connected at different nodes.

**Table 3.** The THD information when three inverters were connected at different buses.

THD (%)	$U_4$	$U_5$	$U_6$	$U_7$	$U_8$	$U_9$
Original case	7.19	5.28	6.18	3.54	4.26	3.77
On Bus 4	3.18	4.87	5.77	3.33	4.00	3.58
On Bus 5	6.46	5.46	5.56	3.41	4.06	3.52
On Bus 6	6.7	4.82	6.51	3.31	4.08	3.52
On Bus 7	6.92	5.07	5.70	3.63	4.33	3.61
On Bus 8	6.81	4.86	5.56	3.52	4.34	3.73
On Bus 9	6.99	5.09	5.83	3.60	4.51	4.71

## 6. Discussion

The proposed scheme has room for improvement and future applications. Three issues identified in this paper are discussed here.

### 6.1. Optimization Objective

The proposed optimization scheme is only suitable for improving the voltage quality, and this is determined by the principle of RMA. If the current quality needs to be improved, the RMA based on loop impedance for analyzing series harmonic resonance needs to be adopted. In addition, for the optimal number of inverters, this paper provides a number range, so this scheme can be combined with the optimization of improving the permeability of the DPG or minimizing power loss.

### 6.2. Improvement of Voltage Quality

Although the optimized THD of bus 4 is already less than 5%, the reader must be aware that the optimized THD has a lower limit, as shown in Figure 15. There are two reasons. One is the reduction in MFS, and the effect of the grid-connected inverter on the harmonic frequency is weakened. The second is that this paper only reduced the 17th harmonic impedance, while the harmonic impedances of other orders were basically maintained.

### 6.3. Target Frequency

The scheme to suppress harmonic amplification proposed in this paper was based on moving the resonance frequency and reducing the harmonic impedance at the harmonic source. However, this measure affects the harmonic impedance of other orders, so the target frequency of the movement needs to be adjusted according to the harmonic source. For example, for a 15th harmonic source in Figure 17, the resonance frequency would need to be shifted further, such as to 700 Hz.

## 7. Conclusions

This paper presented a grid-connected optimization scheme of the inverters to suppress harmonic amplification in a microgrid. This paper first discussed the basic principle of RMA, and then introduced the concepts of PF and MFS. The Norton equivalent circuit model was established and the output impedance of the inverter was evaluated. Furthermore, this paper proved the consistency of the influence of the grid-connection inverter and passive components with the same output impedance on the impedance distribution. In addition, the security region and insecurity region of resonance frequency were illustrated. Then, a harmonic-amplification suppression scheme based on RMA and the grid-connected inverters was proposed. The proposed scheme can significantly reduce the voltage distortion at the resonance center. The originality of the proposed scheme includes: (1) optimized impedance distribution through grid-connected inverters and (2) determination methods of PF-based optimal sites and MFS-based optimal number. The characteristics of the proposed scheme were investigated through simulation verification. Finally, additional applications and improvements of the proposed scheme were discussed.

**Author Contributions:** Conceptualization, X.S. and W.L.; data curation, X.S. and W.L.; formal analysis, Y.D.; methodology, Y.D. and Y.Y.; resources, X.S.; software, W.L.; writing—original draft, X.S.; writing—review and editing, W.L., Y.D., Y.Y. and Q.L.; supervision, Y.D., Y.Y. and Q.L. All authors have read and agreed to the published version of the manuscript.

**Funding:** This work was supported in part by Science and technology plan project of Sichuan Province 2022 YFSY0053.

**Institutional Review Board Statement:** Not applicable.

**Informed Consent Statement:** Not applicable.

**Data Availability Statement:** Not applicable.

**Conflicts of Interest:** The authors declare no conflict of interest.

## References

1. Liu, B.; Liu, Z.; Liu, J.; An, R.; Zheng, H.; Shi, Y. An Adaptive Virtual Impedance Control Scheme Based on Small-AC-Signal Injection for Unbalanced and Harmonic Power Sharing in Islanded Microgrids. *IEEE Trans. Power Electron.* **2019**, *34*, 12333–12355. [[CrossRef](#)]
2. Wei, X.; Li, C.; Qi, M.; Luo, B.; Deng, X.; Zhu, G. Research on Harmonic Current Amplification Effect of Parallel APF Compensating Voltage Source Nonlinear Load. *Energies*. **2019**, *12*, 3070. [[CrossRef](#)]
3. Lou, G.; Yang, Q.; Gu, W.; Quan, X.; Guerrero, J.M.; Li, S. Analysis and Design of Hybrid Harmonic Suppression Scheme for VSG Considering Nonlinear Loads and Distorted Grid. *IEEE Trans. Energy Convers.* **2021**, *36*, 3096–3107. [[CrossRef](#)]
4. Guerrero-Rodríguez, N.F.; Lucas, L.C.H.; de Pablo-Gómez, S.; Rey-Boué, A.B. Performance study of a synchronization algorithm for a 3-phase photovoltaic grid-connected system under harmonic distortions and unbalances. *Electr. Power Syst. Res.* **2014**, *116*, 252–265. [[CrossRef](#)]
5. Smadi, A.A.; Lei, H.; Johnson, K.B. Distribution System Harmonic Mitigation using a PV System with Hybrid Active Filter Features. In Proceedings of the 2019 North American Power Symposium (NAPS), Wichita, KS, USA, 13–15 October 2019; pp. 1–6.
6. Xiao, X.; Li, Z.; Wang, Y.; Zhou, Y. A Practical Approach to Estimate Harmonic Distortions in Residential Distribution System. *IEEE Trans. Power Deliv.* **2021**, *36*, 1418–1427. [[CrossRef](#)]
7. Pereira, J.L.M.; Leal, A.F.R.; Almeida, G.O.D.; Tostes, M.E.D.L. Harmonic Effects Due to the High Penetration of Photovoltaic Generation into a Distribution System. *Energies* **2021**, *14*, 4021. [[CrossRef](#)]
8. Guest, E.; Jensen, K.H.; Rasmussen, T.W. Mitigation of Harmonic Voltage Amplification in Offshore Wind Power Plants by Wind Turbines With Embedded Active Filters. *IEEE Trans. Sustain. Energy* **2020**, *11*, 785–794. [[CrossRef](#)]
9. Nejbatkhah, F.; Li, Y.W.; Wu, B. Control Strategies of Three-Phase Distributed Generation Inverters for Grid Unbalanced Voltage Compensation. *IEEE Trans. Power Electron.* **2016**, *31*, 5228–5241.
10. Herman, L.; Papič, I. Hybrid active filter for power factor correction and harmonics elimination in industrial networks. In Proceedings of the 2011 IEEE Electrical Power and Energy Conference, Winnipeg, MB, Canada, 3–5 October 2011; pp. 302–308.
11. Michalec, Ł.; Jasiński, M.; Sikorski, T.; Leonowicz, Z.; Jasiński, Ł.; Suresh, V. Impact of Harmonic Currents of Nonlinear Loads on Power Quality of a Low Voltage Network—Review and Case Study. *Energies* **2021**, *14*, 3665. [[CrossRef](#)]
12. Wei, L.; Guskov, N.N.; Lukaszewski, R.A.; Skibinski, G.L. Mitigation of Current Harmonics for Multipulse Diode Front-End Rectifier Systems. *IEEE Trans. Ind. Appl.* **2007**, *43*, 787–797. [[CrossRef](#)]

13. Mon-Nzongo, D.L.; Ipoum-Ngome, P.G.; Jin, T.; Song-Manguelle, J. An Improved Topology for Multipulse AC/DC Converters Within HVDC and VFD Systems: Operation in Degraded Modes. *IEEE Trans. Power Electron.* **2018**, *65*, 3646–3656. [[CrossRef](#)]
14. Lai, Z.; Smedley, K.M. A family of continuous-conductionmode power-factor-correction controllers based on the general pulse width modulator. *IEEE Trans. Power Electron.* **1998**, *13*, 501–510.
15. Chou, C.-J.; Liu, C.-W.; Lee, J.-Y.; Lee, K.-D. Optimal planning of large passive-harmonic-filters set at high voltage level. *IEEE Trans. Power Syst.* **2000**, *15*, 433–441. [[CrossRef](#)]
16. Martinek, R.; Rzigly, J.; Jaros, R.; Bilik, P.; Ladrova, M. Least Mean Squares and Recursive Least Squares Algorithms for Total Harmonic Distortion Reduction Using Shunt Active Power Filter Control. *Energies* **2019**, *12*, 1545. [[CrossRef](#)]
17. Zhou, Z.; Li, Y.; Yang, Y.; Huang, X.; Chen, Z. Application of 20 kV high-voltage active power filter (APF). In Proceedings of the 2012 China International Conference on Electricity Distribution, Shanghai, China, 10–14 September 2012; pp. 1–4.
18. Seifossadat, S.G.; Kianinezhad, R.; Ghasemi, A.; Monadi, M. Quality improvement of shunt active power filter, using optimized tuned harmonic passive filters. In Proceedings of the 2008 International Symposium on Power Electronics, Electrical Drives, Automation and Motion, Ischia, Italy, 11–13 June 2008; pp. 1388–1393.
19. Wang, X.; Blaabjerg, F.; Loh, P.C. Grid-Current-Feedback Active Damping for LCL Resonance in Grid-Connected Voltage-Source Converters. *IEEE Trans. Ind. Electron.* **2016**, *31*, 213–223. [[CrossRef](#)]
20. Li, Z.; Hu, H.; Wang, Y.; Tang, L.; He, Z.; Gao, S. Probabilistic Harmonic Resonance Assessment Considering Power System Uncertainties. *IEEE Trans. Power Deliv.* **2018**, *33*, 2989–2998. [[CrossRef](#)]
21. Bouhouras, A.S.; Marinopoulos, A.G.; Labridis, D.P.; Dokopoulos, P.S. Installation of PV systems in Greece—Reliability improvement in the transmission and distribution system. *Electr. Power Syst. Res.* **2010**, *80*, 547–555. [[CrossRef](#)]
22. Belenguer, E.; Beltran, H.; Aparicio, N. Distributed generation power inverters as shunt active power filters for losses minimization in the distribution network. In Proceedings of the 2007 European Conference on Power Electronics and Applications, Aalborg, Denmark, 2–5 September 2007; pp. 1–10.
23. Aghaebrahimi, M.R.; Amiri, M.; Zahiri, S.H. An immune-based optimization method for distributed generation placement in order to minimize power losses. In Proceedings of the 2009 International Conference on Sustainable Power Generation and Supply, Nanjing, China, 6–7 April 2009; pp. 1–6.
24. Chang, C.; Gorinevsky, D.; Lall, S. Dynamical and Voltage Profile Stability of Inverter-Connected Distributed Power Generation. *IEEE Trans. Smart Grid.* **2014**, *5*, 2093–2105. [[CrossRef](#)]
25. Shaheen, A.M.; Elsayed, A.M.; Ginidi, A.R.; El-Sehiemy, R.A.; Elattar, E. A heap-based algorithm with deeper exploitative feature for optimal allocations of distributed generations with feeder reconfiguration in power distribution networks. *Knowl.-Based Syst.* **2022**, *241*, 108269. [[CrossRef](#)]
26. Tu, Y.; Liu, J.; Liu, T.; Cheng, X. Impedance-Based Stability Analysis of Large-Scale PV Station under Weak Grid Condition Considering Solar Radiation Fluctuation. In Proceedings of the 2018 International Power Electronics Conference (IPEC-Niigata 2018—ECCE Asia), Niigata, Japan, 20–24 May 2018; pp. 3934–3939.
27. Teng, J.; Chang, C. Backward/Forward Sweep-Based Harmonic Analysis Method for Distribution Systems. *IEEE Trans. Power Deliv.* **2007**, *22*, 1665–1672. [[CrossRef](#)]
28. Xu, W.; Huang, Z.; Cui, Y.; Wang, H. Harmonic resonance mode analysis. *IEEE Trans. Power Deliv.* **2005**, *20*, 1182–1190. [[CrossRef](#)]
29. He, Z.; Hu, H.; Zhang, Y.; Gao, S. Harmonic Resonance Assessment to Traction Power-Supply System Considering Train Model in China High-Speed Railway. *IEEE Trans. Power Deliv.* **2014**, *29*, 1735–1743. [[CrossRef](#)]
30. Cui, Y.; Wang, X. Modal Frequency Sensitivity for Power System Harmonic Resonance Analysis. *IEEE Trans. Power Deliv.* **2012**, *27*, 1010–1017. [[CrossRef](#)]
31. Sauer, P.W.; Pai, M.A. *Power System Dynamics and Stability*; IEEE Press: New York, NY, USA, 1998; pp. 277–282.